

# False Data Injection Attacks and Corresponding Countermeasure in DC Microgrid <sup>★</sup>

Mengxiang Liu, Peng Cheng, Chengcheng Zhao, Ruilong Deng, Wenhai Wang,  
Jiming Chen

*State Key Lab. of Industrial Control Technology, Zhejiang University, Hangzhou*

---

## Abstract

In this paper, we consider a hierarchical control based DC microgrid (DCmG) equipped with unknown input observer (UIO) based detectors, and investigate false data injection (FDI) attacks against the secondary control layer. First, we point out that the fundamental limitation of the UIO-based detector comes from the unknown inputs, which can be utilized to construct zero trace undetectable (ZTU) attacks causing zero impact on detection residuals. Furthermore, we extend ZTU attacks to nonzero trace undetectable (NTU) attacks by utilizing system noise, under which the detection residuals are still bounded by certain detection thresholds. Then, analytical expressions of the point of common coupling (PCC) voltages are obtained to analyze the impacts of NTU attacks in the DCmG. Moreover, we provide a possible countermeasure against ZTU and NTU attacks by observing the average PCC voltage deviation. Finally, extensive simulations are conducted in Simulink/PLECS to validate theoretical results and effectiveness of the countermeasure.

*Key words:* DC Microgrid; UIO-based detector; ZTU attack; NTU attack; Countermeasure.

---

## 1 Introduction

During the past decades, the microgrid, which is composed of DGUs, storage devices, and flexible loads, has become the most promising solution to integrate distributed generation units (DGUs) such as photovoltaic (PV) arrays and wind turbines into distribution networks [2]. Recently, tremendous growth in DC loads such as laptop computers, LED lights, and telecommunication centers indicates that the DC microgrid (DCmG) can be a economic and feasible solution in addressing the future energy needs.

Generally, a hierarchical control framework is adopted in the DCmG. In primary control layer, the basic control problem is to track local reference voltage [3]. In secondary control layer, each DGU's reference voltage

is regulated based on centralized/distributed communication network to achieve current sharing and voltage balancing [4, 5]. However, communication networks will also expose new attack surfaces to malicious attackers, which can cause economic losses and even crash the DCmG. Meanwhile, due to the novel characteristics of low-inertial DGUs [6], hierarchical control framework [4], and flexible network topology [7], the cyber security of DCmG has attracted considerable attention.

Considering the cyber attacks injecting invalid commands or erroneous measurements into the communication links, Liu *et al.* proposed a resilient decentralized secondary frequency control method for microgrids [8]. And Lu *et al.* designed a distributed strategy to detect the malicious constant signals, by checking the dual-ascent update iterations in micorgrids [9]. Moreover, Beg *et al.* proposed a framework to detect the cyber attacks compromising global variables randomly, by using the candidate invariants in DCmGs [10]. And the unknown input observers (UIOs), which can observer system states regardless of the unknown inputs, are widely adopted to detect and identify malicious nodes/links in unreliable networks [11]. Recently, a novel UIO-based detector is proposed to detect and identify specific cyber attacks in DCmGs [12], where each DGU estimates neighbors' states and requires only neighbors' model

---

<sup>★</sup> This paper was presented in part at the American Control Conference, Philadelphia, PA, July, 2019 [1]. Corresponding author: Peng Cheng

*Email addresses:* lmx329@zju.edu.cn (Mengxiang Liu), pcheng@iipc.zju.edu.cn (Peng Cheng), zccsq90@gmail.com (Chengcheng Zhao), dengruilong@zju.edu.cn (Ruilong Deng), zdzzlab@zju.edu.cn (Wenhai Wang), cjm@zju.edu.cn (Jiming Chen).

parameters and outputs.

However, most existing works assume that attackers have little knowledge of the system model (plant / control/detection parameters). Actually, intelligent attackers can learn critical system parameters after penetrating into the system, and launch attacks at appropriate time coordinately, which can cause devastating damage such as the Stuxnet [13]. Therefore, it is necessary to investigate what the attackers can do when they have some model knowledge of the DCmG, which can provide novel design insights to mitigate potential security threats in DCmGs.

In this paper, we make an effort to explore potential FDI attacks under the UIO-based detector in the DCmG [12]. Compared to previous work [1], we provide comprehensive characterization of FDI attacks and corresponding countermeasure in the DCmG, and main contributions are listed as follows: First, we characterize zero trace undetectable (ZTU) and nonzero trace undetectable (NTU) attacks under the UIO-based detector. Then, by approximating primary control loops as static unit gains [4], we theoretically analyze the attack impacts on current sharing and voltage balancing in the DCmG. Finally, we provide corresponding countermeasure against ZTU and NTU attacks based on the average point of common coupling (PCC) voltage deviation.

The rest of this paper is organized as follows. Section 2 presents the DCmG model and section 3 shows the problem formulation. Then, undetectable attacks under the UIO-based detector are characterized in section 4 and the attack impacts in the DCmG are analyzed in section 5. And corresponding countermeasure is given in section 6. Finally, extensive simulations are presented in Section 7 and Section 8 concludes this paper.

## 2 DCmG Model

**Notation:** In this paper,  $|\cdot|$  calculates the cardinality of finite set and component-by-component absolute value of a matrix/vector,  $\|\cdot\|$  calculates the norm of a matrix/vector, inequalities of matrices/vectors are compared component-by-component, and  $y(\infty) = \lim_{t \rightarrow \infty} y(t)$ .  $\mathbb{1}^n / \mathbb{1}^{n \times n}$  and  $\mathbb{0}^n / \mathbb{0}^{n \times n}$  denote vectors/matrices with all 1 and 0 entries, respectively, and  $\mathbf{I}^n$  denotes the unit matrix with  $n \times n$  dimension. Moreover,  $\mathbb{H}^1$  denotes the subspace of  $\mathbb{R}^n$  composed by all vectors satisfying  $\langle \mathbf{v} \rangle = \frac{1}{n} \sum_{i=1}^n v_i = 0$ , where  $\langle \mathbf{v} \rangle$  denotes the average of all entries in vector  $\mathbf{v}$ . Obviously, each vector in  $\mathbb{H}^1$  has  $n - 1$  freedom<sup>1</sup>, indicating that the dimension of  $\mathbb{H}^1$  is  $n - 1$ , i.e.,  $\dim\{\mathbb{H}^1\} = n - 1$ . The orthogonal subspace of  $\mathbb{H}^1$  is represented by  $\mathbb{H}_\perp^1$ , satisfying  $\mathbf{v} = \alpha \mathbf{1}^n, \alpha \in \mathbb{R}, \forall \mathbf{v} \in \mathbb{H}_\perp^1$ , and  $\dim\{\mathbb{H}_\perp^1\} = 1$ . And  $\mathbb{R}^n$  can be decomposed as  $\mathbb{H}^1 \oplus \mathbb{H}_\perp^1$ , where  $\oplus$  calculates the direct sum of subspaces.

<sup>1</sup> Any  $n - 1$  entries in the vector can be set arbitrarily.

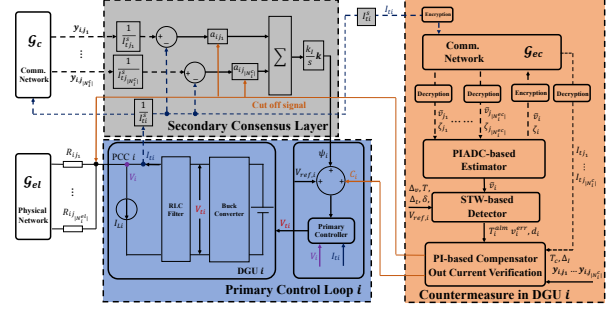


Fig. 1. This figure shows the hierarchical control framework of DGU  $i$ , where the secondary consensus layer and the primary control loop are emphasized in blue and gray shadows, respectively, and corresponding countermeasure is emphasized in orange shadow.

### 2.1 Network Models

A weighted directed graph (digraph) is denoted by  $\mathcal{G} = \{\nu, \varepsilon, \mathbf{W}\}$ , where  $\nu = \{1, 2, \dots, n\}$  is the set of nodes,  $\varepsilon \subseteq \nu \times \nu$  is the set of edges, and the diagonal matrix  $\mathbf{W} = \text{diag}\{a_{ij}\} \in \mathbb{R}^{|\varepsilon| \times |\varepsilon|}$ .  $a_{ij}$  is the weight of edge  $(i, j) \in \varepsilon$  and the set of neighbors of node  $i$  is  $\mathcal{N}_i = \{j | (i, j) \in \varepsilon \text{ or } (j, i) \in \varepsilon\}$ . The Laplacian matrix of  $\mathcal{G}$  is  $\mathcal{L}(\mathcal{G})$ , which is independent of the orientations of edges.

**Electrical and Communication Networks:** The electrical network of DCmG is represented by  $\mathcal{G}_{el} = \{\nu, \varepsilon_{el}, \mathbf{W}_{el}\}$ , where nodes are the DGUs, edges are the power lines whose orientations define the reference directions of positive currents, and the weights are the conductances of power lines, i.e.,  $1/R_{ij}$ . Moreover, the set of neighbors of node  $i$  is  $\mathcal{N}_i^{el}$ ,  $|\nu| = N$  and  $\mathcal{L}(\mathcal{G}) = \mathbf{M}$ . The unencrypted (encrypted) bidirectional communication network of DCmG is denoted by  $\mathcal{G}_c = \{\nu, \varepsilon_c, \mathbf{W}_c\}$  ( $\mathcal{G}_{ec} = \{\nu, \varepsilon_{ec}, \mathbf{W}_{ec}\}$ ), where the weight  $a_{ij}^c = a_{ji}^c$  ( $a_{ij}^{ec} = a_{ji}^{ec}$ ) and  $a_{ij}^c > 0$  ( $a_{ij}^{ec} > 0$ ) if edge  $(i, j) \in \varepsilon_c$  ( $(i, j) \in \varepsilon_{ec}$ ). The set of neighbors of node  $i$  is  $\mathcal{N}_i^c$  ( $\mathcal{N}_i^{ec}$ ), and  $\mathcal{L}(\mathcal{G}_c) = \mathbf{L}$  ( $\mathcal{L}(\mathcal{G}_{ec}) = \mathbf{L}_e$ ).

**Assumption 1:** The digraphs  $\mathcal{G}_c$  and  $\mathcal{G}_{el}$  are weakly connected<sup>2</sup>. Moreover,  $\mathcal{G}_c$  and  $\mathcal{G}_{el}$  have the same topology, and  $\mathbf{L} = \mathbf{M}$ .

**Assumption 2:** The digraph  $\mathcal{G}_{ec}$  is weakly connected and  $\varepsilon_c \subseteq \varepsilon_{ec}$ .

**Remark 1:** Assumption 1 is established to guarantee globally exponentially stable control of DCmG according to [4], under which DGU  $i$  need know the resistances  $R_{ij}$  of all power lines connecting it to its electrical neighbors  $j, j \in \mathcal{N}_i^{el}$ . Given the quasi-stationary line approximations of power line dynamics [3],  $R_{ij}$  can be estimated through  $R_{ij} = \frac{|V_j - V_i|}{I_{ij}}$  in steady state, where  $I_{ij}$  is the current on power line  $(i, j)$ ,  $V_i$  and  $I_{ij}$  are measured by DGU  $i$  locally, and  $V_j$  is transmitted from DGU  $j$  to  $i$  over  $\mathcal{G}_{ec}$ . Moreover, Assumption 2 gives some basic properties of  $\mathcal{G}_{ec}$  to make the countermeasure effective.

<sup>2</sup> A directed graph is weakly connected if replacing all of its directed edges with undirected edges produces a connected graph.

## 2.2 Dynamics Model

According to Fig.1, each DGU contains a DC voltage source, a buck converter, a local load current and a RLC (resistor, inductor, and capacitor) filter, where  $V_{ii}$  is the output voltage of DC buck converter,  $I_{Li}$  is the load current, and  $V_i$  and  $I_{ti}$  are the PCC voltage and the output current, respectively. Hierarchical control framework is deployed in each DGU, where primary controller tracks local reference voltage and secondary consensus layer regulates local reference voltage to achieve current sharing and voltage balancing in the DCmG [4]. The dynamics model of DGU  $i$  is

$$\begin{cases} \dot{\mathbf{x}}_i(t) = \mathbf{A}_{ii}\mathbf{x}_i(t) + \mathbf{b}_i u_i(t) + \mathbf{g}_i \psi_i(t) + \\ \quad + \mathbf{M}_i \mathbf{d}_i + \boldsymbol{\xi}_i(t) + \boldsymbol{\omega}_i(t) \\ \mathbf{y}_i(t) = \mathbf{C}_i \mathbf{x}_i(t) + \boldsymbol{\rho}_i(t) \end{cases}, \quad (1)$$

where  $\mathbf{x}_i(t) = [V_i(t), I_{ti}(t), v_i(t)]^T$  is the state vector.  $v_i(t)$  is the integral of voltage tracking error satisfying  $\dot{v}_i(t) = V_{ref,i} + \psi_i(t) - V_i(t)$ , where  $V_{ref,i}$  is the nominal reference voltage of DGU  $i$  and  $\psi_i(t)$  is the secondary input. Besides,  $\mathbf{d}_i = [I_{Li}, V_{ref,i}]^T$  is constant exogenous input vector,  $\mathbf{y}_i(t) \in \mathbb{R}^3$  denotes the output vector and  $\mathbf{C}_i = \mathbf{I}^3$ . The physical couplings with neighbor DGUs are modeled as  $\boldsymbol{\xi}_i(t) = \sum_{j \in \mathcal{N}_i^c} \mathbf{A}_{ij} \mathbf{x}_j(t) \in \mathbb{R}^3$ , and details of  $\mathbf{A}_{ii}$ ,  $\mathbf{A}_{ij}$ ,  $\mathbf{M}_i$ ,  $\mathbf{g}_i$ ,  $\mathbf{b}_i$  can be found in [3]. We assume the process noise and measurement noise satisfy the following assumption:

**Assumption 3:** The process noise and measurement noise are unknown-but-bounded (UBB) i.e.,  $|\boldsymbol{\omega}_i(t)| \leq \bar{\boldsymbol{\omega}}_i \in \mathbb{R}^3$ ,  $|\boldsymbol{\rho}_i(t)| \leq \bar{\boldsymbol{\rho}}_i \in \mathbb{R}^3$ ,  $\forall t \geq 0$ .

**Remark 2:** There exists several practical situations where the noise is UBB. For example, the noise during the audio design is a set of narrow-band signals with frequency spectrum range from 20HZ to 20KHZ [14]. And the bounds of noise are related to the bounds of parameter variation and sensor's quantization error [15].

The primary control input is  $u_i(t) = V_{ti} = \mathbf{k}_i^T \mathbf{y}_i(t)$ , where  $\mathbf{k}_i \in \mathbb{R}^3$  depends only on local information [3]. The secondary control input is obtained through the following consensus scheme:

$$\dot{\psi}_i(t) = -[0, k_I, 0] \sum_{j \in \mathcal{N}_i^c} a_{ij}^c \left( \frac{\mathbf{y}_i(t)}{I_{ti}^s} - \frac{\mathbf{y}_{i,j}(t)}{I_{tj}^s} \right), \quad (2)$$

where  $\mathbf{y}_{i,j}^c(t) \in \mathbb{R}^3$  is the output of DGU  $j$  transmitted to DGU  $i$  over  $\mathcal{G}_c$ ,  $I_{ti}^s > 0$ ,  $I_{tj}^s > 0$  are corresponding rated currents, and  $k_I > 0$  is a parameter invariant among  $\mathcal{E}_c$ . Without loss of generality, we assume the nominal reference voltages satisfy Assumption 4 as in [4]:

**Assumption 4:** The nominal reference voltages are equal among all DGUs, i.e.,  $V_{ref,i} = V_{ref}$ ,  $\forall i \in \nu$ .

**Definition 1 (Voltage Balancing):** Under Assumption 4, voltage balancing is achieved if  $\langle v(\infty) \rangle = V_{ref}$ , where  $\langle v(\infty) \rangle$  is the steady state average PCC voltage.

**Definition 2 (Current Sharing):** For constant load currents, current sharing is achieved if  $\frac{I_{ti}(\infty)}{I_{ti}^s} = \frac{I_{tj}(\infty)}{I_{tj}^s}$ ,  $\forall i, j \in \nu$ , i.e., load currents are shared proportionally to DGUs' rated currents.

## 3 Problem Formulation

### 3.1 Attack Model

We consider the FDI attacks injecting malicious signals into communication links, which is modeled as

$$\mathbf{y}_{i,j}^c(t) = \mathbf{y}_j(t) + \tau(t - T_a) \boldsymbol{\phi}_{i,j}(t), \quad (3)$$

where  $\mathbf{y}_{i,j}^c(t)$  is the corrupted data that DGU  $i$  receives from DGU  $j$  through link  $(i, j) \in \mathcal{E}_c$ ,  $\boldsymbol{\phi}_{i,j}(t)$  is the attack vector and  $\tau(t - T_a)$  is the step function with  $T_a$  delay. Obviously, the attack is started at  $t = T_a$ , and  $\mathbf{y}_{i,j}^c(t) = \mathbf{y}_j(t)$ ,  $t \leq T_a$ . Furthermore, the attacker can get some static plant/control/detection parameters of each DGU from insiders, but is hard to intrude into DGUs due to various host-based defense mechanisms [16], e.g., the firewalls.

### 3.2 UIO-based Detector

A bank of UIO-based detectors is deployed in each DGU to detect and identify the FDI attack (3) according to [12]. First, we transform the dynamics model of DGU  $j$ ,  $j \in \mathcal{N}_i^c$  to the typical UIO structure:

$$\begin{cases} \dot{\mathbf{x}}_j(t) = \mathbf{A}_{kj} \mathbf{x}_j(t) + \bar{\mathbf{E}}_j \bar{\mathbf{d}}_j(t) + \boldsymbol{\omega}_j(t) + \mathbf{b}_j \mathbf{k}_j \boldsymbol{\rho}_j(t) \\ \mathbf{y}_j(t) = \mathbf{C}_j \mathbf{x}_j(t) + \boldsymbol{\rho}_j(t) \end{cases}, \quad (4)$$

where  $\mathbf{A}_{kj} = \mathbf{A}_{jj} + \mathbf{b}_j \mathbf{k}_j^T \in \mathbb{R}^{3 \times 3}$ ,  $\bar{\mathbf{E}}_j \bar{\mathbf{d}}_j(t) = \mathbf{M}_j \mathbf{d}_j + \mathbf{g}_j \psi_j(t) + \boldsymbol{\xi}_j(t)$ ,  $\bar{\mathbf{d}}_j(t) \in \mathbb{R}^2$  denotes the unknown inputs to DGU  $i$ , and  $\bar{\mathbf{E}}_j \in \mathbb{R}^{3 \times 2}$  is a known parameter related to the capacitor parameter  $C_{tj}$ :

$$\bar{\mathbf{E}}_j = \begin{bmatrix} \frac{1}{C_{tj}} & 0 & 0 \\ 0 & 0 & 1 \end{bmatrix}^T, \mathbf{H}_j = \begin{bmatrix} 1 & 0 & 0 \\ h_{12} & h_{22} & h_{32} \\ 0 & 0 & 1 \end{bmatrix}. \quad (5)$$

According to Theorem 1 in [17], we can construct the full order UIO deployed in DGU  $i$  as  $\mathbf{C}_j = \mathbf{I}^3$ :

$$\begin{cases} \dot{\mathbf{z}}_{i,j}(t) = \mathbf{F}_j \mathbf{z}_{i,j}(t) + \hat{\mathbf{K}}_j \mathbf{y}_{i,j}^c(t) \\ \hat{\mathbf{x}}_{i,j}(t) = \mathbf{z}_{i,j}(t) + \mathbf{H}_j \mathbf{y}_{i,j}^c(t) \end{cases}, \quad (6)$$

under which the state estimation error decays exponentially to a certain range related to system noise regardless of the unknown inputs  $\bar{\mathbf{d}}_j(t)$ .  $\mathbf{z}_{i,j}(t) \in \mathbb{R}^3$  is the state vector of the UIO,  $\hat{\mathbf{x}}_{i,j}(t)$  is the estimated state of DGU  $j$ , and the UIO parameters  $\mathbf{F}_j, \hat{\mathbf{K}}_j, \mathbf{H}_j \in \mathbb{R}^{3 \times 3}$  satisfy

$$\begin{cases} \hat{\mathbf{K}}_j = \mathbf{K}_1 + \mathbf{K}_2, \mathbf{T}_j = \mathbf{I}^3 - \mathbf{H}_j \\ \mathbf{T}_j \bar{\mathbf{E}}_j = \mathbf{0}^{3 \times 2}, \mathbf{F}_j = \mathbf{T}_j \mathbf{A}_{kj} - \mathbf{K}_1, \mathbf{K}_2 = \mathbf{F}_j \mathbf{H}_j \end{cases}, \quad (7)$$

where  $\mathbf{K}_1, \mathbf{K}_2, \mathbf{T}_j \in \mathbb{R}^{3 \times 3}$ ,  $\mathbf{H}_j$  is defined in (5), and  $h_{12}, h_{22}, h_{32} \in \mathbb{R}$ . Note that  $\mathbf{K}_1$  should be appropriately chosen to make  $\mathbf{F}_j$  stable, and (7) is determined once  $\mathbf{H}_j$  and  $\mathbf{K}_1$  are given. Let  $\boldsymbol{\epsilon}_{i,j}(t) = \mathbf{x}_j(t) - \hat{\mathbf{x}}_{i,j}(t)$  and  $\mathbf{r}_{i,j}(t) = \boldsymbol{\epsilon}_{i,j}(t) + \boldsymbol{\rho}_j(t)$  be the state estimation error and detection residual of (6), respectively, in the absence of attacks. And analytical expression of  $\mathbf{r}_{i,j}(t)$  is

$$\mathbf{r}_{i,j}(t) = e^{\mathbf{F}_j t}(\boldsymbol{\sigma}_{i,j}^2(0) + \boldsymbol{\sigma}_{i,j}^3(t)) + \mathbf{T}_j \boldsymbol{\rho}_j(t),$$

where  $\boldsymbol{\sigma}_{i,j}^2(0) = \boldsymbol{\epsilon}_{i,j}(0) + \mathbf{H}_j \boldsymbol{\rho}_j(0)$  and  $\boldsymbol{\sigma}_{i,j}^3(t) = \int_0^t e^{-\mathbf{F}_j \tau} (\mathbf{T}_j \boldsymbol{\omega}_j(\tau) + (\mathbf{T}_j \mathbf{b}_j \mathbf{k}_j - \hat{\mathbf{K}}_j) \boldsymbol{\rho}_j(\tau)) d\tau$ . And the initial state estimation error  $\boldsymbol{\epsilon}_{i,j}(0)$  can be bounded into the bound of measurement noise as  $\mathbf{C}_j = \mathbf{I}^3$ , i.e.,  $|\boldsymbol{\epsilon}_{i,j}(0)| \leq \bar{\boldsymbol{\rho}}_j$ . Moreover, there always exists positive constants  $\kappa, \mu$  such that  $\|e^{\mathbf{F}_j t}\| \leq \kappa e^{-\mu t}$  as  $\mathbf{F}_j$  is stable. Then, the upper bound of  $|\mathbf{r}_{i,j}(t)|$  is

$$\bar{\mathbf{r}}_{i,j}(t) = \kappa e^{-\mu t} (\bar{\boldsymbol{\sigma}}_{i,j}^2(0) + \bar{\boldsymbol{\sigma}}_{i,j}^3(t)) + |\mathbf{T}_j| \bar{\boldsymbol{\rho}}_j, \quad (8)$$

where  $|\boldsymbol{\sigma}_{i,j}^2(0)| \leq \bar{\boldsymbol{\sigma}}_{i,j}^2(0) = (\mathbf{I}^3 + |\mathbf{H}_j|) \bar{\boldsymbol{\rho}}_j$ ,  $|\boldsymbol{\sigma}_{i,j}^3(t)| \leq \bar{\boldsymbol{\sigma}}_{i,j}^3(t) = \int_0^t |e^{-\mathbf{F}_j \tau}| (|\mathbf{T}_j| \bar{\boldsymbol{\omega}}_j + |\mathbf{T}_j \mathbf{b}_j \mathbf{k}_j - \hat{\mathbf{K}}_j| \bar{\boldsymbol{\rho}}_j) d\tau$ . As  $\bar{\boldsymbol{d}}_j(t)$  contains the load current and physical couplings, daily operations such as load switches and plugging-in/out of DGUs will not affect  $\mathbf{r}_{i,j}(t)$ . Therefore, once

$$|\mathbf{r}_{i,j}(t)| \geq \bar{\mathbf{r}}_{i,j}(t), \quad (9)$$

it is assumed that  $\mathbf{y}_{i,j}^c(t)$  is corrupted by FDI attack (3). And false alarm and missed alarm under the UIO-based detector are formally defined as follows.

**Definition 3:** If (9) is triggered when there exists no FDI attack (3), then it is called a **False Alarm**; If (9) is not triggered when there exists FDI attack (3), then it is called a **Missed Alarm**.

### 3.3 Problems of Interest

Although zero false alarm can be achieved under the UIO-based detector (6) and the trigger condition (9), zero missed alarm cannot be guaranteed simultaneously. In another word, there exists some undetectable attacks. First, we characterize the detection residual under attack (3) as  $\tilde{\mathbf{r}}_{i,j}(t) = \mathbf{r}_{i,j}(t) + \mathbf{r}_{i,j}^a(t)$ , where

$$\begin{aligned} \mathbf{r}_{i,j}^a(t) = & e^{\mathbf{F}_j(t-T_a)} \mathbf{H}_j \boldsymbol{\phi}_{i,j}(T_a) + \mathbf{T}_j \boldsymbol{\phi}_{i,j}(t) + \\ & - \int_{T_a}^t e^{\mathbf{F}_j(t-\tau)} \hat{\mathbf{K}}_j \boldsymbol{\phi}_{i,j}(\tau) d\tau. \end{aligned} \quad (10)$$

On the one hand, (9) can be immediately triggered once  $|\mathbf{r}_{i,j}^a(t)| > 2\bar{\mathbf{r}}_{i,j}(t)$  [12]; On the other hand, the FDI attack (3) is undetectable if and only if  $|\tilde{\mathbf{r}}_{i,j}(t)| \leq \bar{\mathbf{r}}_{i,j}(t)$ . Moreover, since  $\mathbf{C}_j = \mathbf{I}^3$ , there exists no invariant zero in (4) according to Definition 4.4.1 in [18], indicating the absence of zero dynamics. Therefore, distinguished from the zero dynamics attack in [19], we aim to further explore undetectable FDI attacks (3) under the characteristics of the UIO-based detector in this paper. According to zero/nonzero  $\mathbf{r}_{i,j}^a(t)$ , we divide the undetectable FDI attacks into the following two forms:

**Definition 4:** The FDI attack (3) is **Zero Trace Undetectable (ZTU)** if

$$\tilde{\mathbf{r}}_{i,j}(t) = \mathbf{r}_{i,j}(t), \boldsymbol{\phi}_{i,j}(t) \neq \mathbf{0}^3. \quad (11)$$

**Definition 5:** The FDI attack (3) is **Nonzero Trace Undetectable (NTU)** if

$$\tilde{\mathbf{r}}_{i,j}(t) \neq \mathbf{r}_{i,j}(t), |\tilde{\mathbf{r}}_{i,j}(t)| \leq \bar{\mathbf{r}}_{i,j}(t), \boldsymbol{\phi}_{i,j}(t) \neq \mathbf{0}^3. \quad (12)$$

And we aim to solve the following three problems in this paper: (1) How to characterize the undetectable attacks (3) under the UIO-based detector (ZTU and NTU attacks)? (**P1**); (2) How will the possible undetectable FDI attacks affect the DCmG? (**P2**); How to counteract the possible undetectable FDI attacks in the DCmG? (**P3**).

## 4 Undetectable Attacks under UIO-based Detector

In this section, we characterize the undetectable attacks under the UIO-based detector (6) given the typical UIO form (4). Obviously, the UIO-based detector cannot distinguish the malicious data mimicking the dynamics of unknown inputs in (4) from normal measurement, and thus we have

**Theorem 1:** If and only if

$$\begin{cases} \dot{\mathbf{x}}_j^a(t) = \mathbf{A}_{kj} \mathbf{x}_j^a(t) + \bar{\mathbf{E}}_j \bar{\mathbf{d}}_j^a(t) \\ \boldsymbol{\phi}_{i,j}(t) = \mathbf{x}_j^a(t), \mathbf{x}_j^a(T_a) = \mathbf{0}^3, \bar{\mathbf{d}}_j^a(t) \neq \mathbf{0}^2, \end{cases} \quad (13)$$

for  $t \geq T_a$ , where  $\mathbf{x}_j^a(t) \in \mathbb{R}^3$ , then the attack (3) is ZTU.

**Proof:** (If) According to (4), the Laplace form of  $\mathbf{y}_{i,j}^c(t)$  under (13) is

$$\begin{aligned} \mathbf{y}_{i,j}^c(s) = & (s\mathbf{I}^3 - \mathbf{A}_{kj})^{-1} (\mathbf{x}_j(0) + \bar{\mathbf{E}}_j \bar{\mathbf{d}}_j(s) + \\ & + \boldsymbol{\omega}_j(s) + \mathbf{b}_j \mathbf{k}_j \boldsymbol{\rho}_j(s)) + \boldsymbol{\rho}_j(s), \end{aligned} \quad (14)$$

where  $s$  is the Laplacian and  $\bar{\mathbf{d}}_j(s) = \bar{\mathbf{d}}_j(s) + \bar{\mathbf{d}}_j^a(s)$ . Obviously, (14) is equivalent to the output of (4) where the unknown input  $\bar{\mathbf{d}}_j(t)$  is switched to  $\bar{\mathbf{d}}_j^a(t)$  at  $t = T_a$ . Since the detection residual of the UIO-based detector is invariant regardless of the unknown input, the attack satisfying (13) is ZTU.

(Only If) According to the definition of ZTU attack (11), we get

$$\mathbf{r}_{i,j}^a(T_a) = \mathbf{0}^3, \dot{\mathbf{r}}_{i,j}^a(t) = \mathbf{0}^3, \forall t \geq T_a. \quad (15)$$

Given  $\mathbf{r}_{i,j}^a(T_a) = \mathbf{0}^3$  and (10), we get  $(\mathbf{H}_j + \mathbf{T}_j) \boldsymbol{\phi}_{i,j}(T_a) = \mathbf{0}^3$ . And  $\mathbf{H}_j + \mathbf{T}_j = \mathbf{I}^3$  according to (7), indicating that  $\boldsymbol{\phi}_{i,j}(T_a) = \mathbf{0}^3$ . After substituting  $\boldsymbol{\phi}_{i,j}(T_a) = \mathbf{0}^3$  into (10), we can transform  $\dot{\mathbf{r}}_{i,j}^a(t) = \mathbf{0}^3$  into

$$\mathbf{T}_j \dot{\boldsymbol{\phi}}_{i,j}(t) = (\mathbf{F}_j \mathbf{T}_j + \hat{\mathbf{K}}_j) \boldsymbol{\phi}_{i,j}(t). \quad (16)$$

Moreover, as  $\mathbf{T}_j \bar{\mathbf{E}}_j = \mathbf{0}^{3 \times 2}$  and  $\text{rank}(\mathbf{T}_j) + \text{rank}(\bar{\mathbf{E}}_j) = 3$ , the image of  $\bar{\mathbf{E}}_j$  is consistent with the null space of  $\mathbf{T}_j$ . Meanwhile, according to (7), we have  $\mathbf{T}_j \mathbf{A}_{kj} = \mathbf{F}_j \mathbf{T}_j + \hat{\mathbf{K}}_j$ . Therefore, the solution of (15) is equivalent to (13), which completes the proof. ■

By extending ZTU attack (13) to nonzero initial state case based on system noise in (4), we get the NTU attack:

**Theorem 2:** The FDI attack (3) is NTU if

$$\begin{cases} \dot{\mathbf{x}}_j^a(t) = \mathbf{A}_{kj} \mathbf{x}_j^a(t) + \bar{\mathbf{E}}_j \bar{\mathbf{d}}_j^a(t) \\ \boldsymbol{\phi}_{i,j}(t) = \mathbf{x}_j^a(t) \end{cases}, \quad (17)$$

for all  $t \geq T_a$ ,  $\bar{\mathbf{d}}_j^a(t) \in \mathbb{R}^2$ , and

$$\phi_{i,j}(T_a) = \mathbf{x}_j^a(T_a) = \tilde{\mathbf{I}}^3 e^{\mathbf{F}_j T_a} \tilde{\boldsymbol{\sigma}}_{i,j}(T_a), \quad (18)$$

where nonzero  $\tilde{\boldsymbol{\sigma}}_{i,j}(T_a) \in \mathbb{R}^3$  satisfies  $|e^{-\mathbf{F}_j T_a} \phi_{i,j}(T_a)| \leq \bar{\boldsymbol{\sigma}}_{i,j}^2(0) + \bar{\boldsymbol{\sigma}}_{i,j}^3(T_a)$ , and  $\tilde{\mathbf{I}}^3 \in \mathbb{R}^3$  is derived from the unit matrix  $\mathbf{I}^3$  with its  $(2, 2)_{th}$  diagonal entry replaced by 0. **Proof:** Combining (5), (7) and (18), we get  $\mathbf{T}_j \phi_{i,j}(T_a) = \mathbf{0}^3$ , indicating that (17) and (18) are the solution of  $\mathbf{T}_j \phi_{i,j}(t) = \int_{T_a}^t e^{\mathbf{F}_j(t-\tau)} \hat{\mathbf{K}}_j \phi_{i,j}(\tau) d\tau$ . Moreover, it is inferred from (7) that  $\mathbf{H}_j \phi_{i,j}(T_a) = \phi_{i,j}(T_a)$ . Then, (10) can be transformed to  $\mathbf{r}_{i,j}^a(t) = e^{\mathbf{F}_j(t-T_a)} \phi_{i,j}(T_a)$ . Therefore,

$$\tilde{\mathbf{r}}_{i,j}(t) = e^{\mathbf{F}_j t} (e^{-\mathbf{F}_j T_a} \phi_{i,j}(T_a) + \boldsymbol{\sigma}_{i,j}^2(0) + \boldsymbol{\sigma}_{i,j}^3(t)) + \mathbf{T}_j \boldsymbol{\rho}_j(t).$$

Since  $|\boldsymbol{\sigma}_{i,j}^2(0)| \leq \bar{\boldsymbol{\sigma}}_{i,j}^2(0)$  and  $|\boldsymbol{\sigma}_{i,j}^3(T_a)| \leq \bar{\boldsymbol{\sigma}}_{i,j}^3(T_a)$ , there always exists a nonzero  $\tilde{\boldsymbol{\sigma}}_{i,j}(T_a)$  satisfying  $|e^{-\mathbf{F}_j T_a} \phi_{i,j}(T_a)| \leq \bar{\boldsymbol{\sigma}}_{i,j}^2(0) + \bar{\boldsymbol{\sigma}}_{i,j}^3(T_a)$  such that  $|e^{-\mathbf{F}_j T_a} \phi_{i,j}(T_a) + \boldsymbol{\sigma}_{i,j}^2(0) + \boldsymbol{\sigma}_{i,j}^3(T_a)| \leq \bar{\boldsymbol{\sigma}}_{i,j}^2(0) + \bar{\boldsymbol{\sigma}}_{i,j}^3(T_a)$ . Moreover,  $|\boldsymbol{\sigma}_{i,j}^3(t) - \boldsymbol{\sigma}_{i,j}^3(T_a)| \leq \bar{\boldsymbol{\sigma}}_{i,j}^3(t) - \bar{\boldsymbol{\sigma}}_{i,j}^3(T_a)$ ,  $t \geq T_a$ , and thus

$$|\tilde{\mathbf{r}}_{i,j}(t)| \leq \bar{\mathbf{r}}_{i,j}(t) \leq \bar{\mathbf{r}}_{i,j}(t), t \geq T_a, \quad (19)$$

where  $\bar{\mathbf{r}}_{i,j}(t) = \kappa e^{-\mu t} (|e^{-\mathbf{F}_j T_a} \phi_{i,j}(T_a) + \boldsymbol{\sigma}_{i,j}^2(0) + \boldsymbol{\sigma}_{i,j}^3(T_a)| + |\boldsymbol{\sigma}_{i,j}^3(t) - \boldsymbol{\sigma}_{i,j}^3(T_a)|) + |\mathbf{T}_j| \bar{\boldsymbol{\rho}}_j$  denotes the tighter threshold caused by  $\phi_{i,j}(t)$  satisfying (17) and (18). And thus the FDI attack vector (3) under (17) and (18) is NTU, which completes the proof.  $\blacksquare$

**Remark 3:** In Theorems 1-2, we reveal that the fundamental limitation of the UIO-based detector (6) comes from the unknown input  $\tilde{\mathbf{d}}_j(t)$ , which can be exploited to construct ZTU and NTU attacks. On the one hand, the UIO-based detector (6) can reduce required inputs to estimate its neighbor DGUs' states; On the other hand, it will increase the threats of undetectable attacks. Therefore, the unknown inputs of the UIO-based detector should be appropriately chosen to balance the costs of transmitting inputs and the threats of cyber attacks.

**Remark 4:** The ZTU attack (13) can be arbitrary large as  $(\mathbf{A}_{kj}, \bar{\mathbf{E}}_j)$  is controllable, and the initial state of NTU attack  $\phi_{i,j}(T_a)$  is mainly constrained by  $e^{\mathbf{F}_j T_a} \bar{\boldsymbol{\sigma}}_{i,j}^3(T_a)$ , which is almost invariant with the growth of  $T_a$  when  $T_a$  is big enough.

## 5 Attack Impacts Analysis in the DCmG

In this section, we analyze the impacts of NTU attack (17) in the DCmG, which contains the impacts of ZTU attack (13). Although the NTU attack vector  $\phi_{i,j}(t)$  can be arbitrarily large with well designed  $\tilde{\mathbf{d}}_j^a(t)$  according to Remark 4,  $\tilde{\mathbf{d}}_j^a(t)$  should be bounded to make the corrupted measurement  $\mathbf{y}_{i,j}^c(t)$  physically reachable given the maximal/minimal PCC voltage and output current in each DGU. Therefore, we consider the most common and practical case where  $\tilde{\mathbf{d}}_j^a(t)$  is a bounded constant,

and constant  $\tilde{\mathbf{d}}_j^a(t)$  is simplified as  $\tilde{\mathbf{d}}_j^a$ . Then, the attack vector is

$$\phi_{i,j}(t) = e^{\mathbf{A}_{kj}(t-T_a)} \tilde{\phi}_{i,j}(T_a) - \mathbf{A}_{kj}^{-1} \bar{\mathbf{E}}_j \tilde{\mathbf{d}}_j^a, \quad (20)$$

where  $\tilde{\phi}_{i,j}(T_a) = \phi_{i,j}(T_a) + \mathbf{A}_{kj}^{-1} \bar{\mathbf{E}}_j \tilde{\mathbf{d}}_j^a \in \mathbb{R}^3$ . Under the NTU attacks, we simplify the primary control loops as unit gains according to [4], i.e.,

$$\tilde{\mathbf{v}}(t) = \mathbf{v}_{ref} + \tilde{\boldsymbol{\psi}}(t), \quad (21)$$

where  $\tilde{\mathbf{v}}(t) = [\tilde{V}_1(t), \dots, \tilde{V}_N(t)]^T$  is the PCC voltage vector under attack,  $\mathbf{v}_{ref} = [V_{ref,1}, \dots, V_{ref,N}]^T$  is constant nominal reference PCC voltage vector, and  $\tilde{\boldsymbol{\psi}}(t) = [\tilde{\psi}_1(t), \dots, \tilde{\psi}_N(t)]^T$  is the secondary control input vector under attack. Given (2) and (3), we have

$$\tilde{\boldsymbol{\psi}}(t) = -\tilde{\mathbf{L}} \mathbf{D} \tilde{\mathbf{i}}_t(t) + C_{ij}^a \mathbf{k} \phi_{i,j}(t) \mathbf{l}_i, \quad (22)$$

where  $\tilde{\mathbf{L}} = k_I \mathbf{L}$ ,  $\mathbf{D} = \text{diag}\{\frac{1}{I_{1s}^s}, \dots, \frac{1}{I_{Ns}^s}\}$ ,  $\tilde{\mathbf{i}}_t(t) = [\tilde{I}_{t1}(t), \dots, \tilde{I}_{tN}(t)]^T$  is the output current vector under attack,  $C_{ij}^a = \frac{k_I a_{ij}^c}{I_{ij}^s}$ ,  $\mathbf{k} = [0, 1, 0]$ , and  $\mathbf{l}_i = \tilde{\mathbf{0}}_i^N \in \mathbb{R}^N$  is derived from  $\mathbf{0}^N$  with its  $i_{th}$  entry replaced by 1 to denote the targeted DGU  $i$ . According to the Kirchhoff current law, the output current is decomposed as  $\tilde{\mathbf{i}}_t(t) = \mathbf{M} \tilde{\mathbf{v}}(t) + \mathbf{i}_l$ , where  $\mathbf{i}_l = [I_{L1}, \dots, I_{LN}]^T$  is the constant load current vector. Therefore, combining (21) with (22), we get

$$\tilde{\boldsymbol{\psi}}(t) = -\mathbf{Q} \tilde{\boldsymbol{\psi}}(t) - \tilde{\mathbf{L}} \mathbf{D} \mathbf{i}_l - \mathbf{Q} \mathbf{v}_{ref} + C_{ij}^a \mathbf{k} \phi_{i,j}(t) \mathbf{l}_i, \quad (23)$$

where  $\mathbf{Q} = \tilde{\mathbf{L}} \mathbf{D} \mathbf{M}$ . Similar to the detection residual,  $\tilde{\boldsymbol{\psi}}(t)$  is decomposed as  $\tilde{\boldsymbol{\psi}}(t) = \boldsymbol{\psi}(t) + \boldsymbol{\psi}_a(t)$ , where  $\boldsymbol{\psi}_a(t)$  denotes the attack impacts on  $\boldsymbol{\psi}(t)$ .

**Theorem 3:** Under single NTU attack (20), we get

$$\langle \boldsymbol{\psi}_a(\infty) \rangle = \frac{C_{ij}^a}{N} \mathbf{k} \mathbf{A}_{kj}^{-1} ((t - T_a) \bar{\mathbf{E}}_j \tilde{\mathbf{d}}_j^a - \tilde{\phi}_{i,j}(T_a)). \quad (24)$$

Note that  $\langle \boldsymbol{\psi}_a(t) \rangle$  doesn't converge with  $t$ , indicating that neither voltage balancing nor current sharing can be achieved in the DCmG.

**Proof:** The Proof is given in Appendix A.  $\blacksquare$

Moreover, the attack vectors (20) can be injected into multi-links  $\tilde{\boldsymbol{\epsilon}}_a \subseteq \boldsymbol{\epsilon}_c$  cooperatively to eliminate the unstable element in (24). Given the linear dynamics of (23), the impacts caused by compromising multi-links are the sum of the impacts that would have been caused by compromising each link individually. Therefore, the impacts of cooperative NTU attacks are characterized as

**Theorem 4:** If multi-links  $\tilde{\boldsymbol{\epsilon}}_a$  are compromised by NTU attacks (20) cooperatively and the attack vectors satisfy

$$\sum_{(i,j) \in \tilde{\boldsymbol{\epsilon}}_a} C_{ij}^a \mathbf{k} \phi_{i,j}(\infty) = 0, \quad (25)$$

then voltage balancing is achieved if  $\sum_{(i,j) \in \tilde{\boldsymbol{\epsilon}}_a} \frac{C_{ij}^a}{N} \mathbf{k} \mathbf{A}_{kj}^{-1} \tilde{\phi}_{i,j}(T_a) = 0$  and current sharing is achieved if  $\sum_{(i,j) \in \tilde{\boldsymbol{\epsilon}}_a} C_{ij}^a \mathbf{k} \phi_{i,j}(\infty) \mathbf{l}_i = \mathbf{0}^N$ .

**Proof:** The Proof is given in Appendix B.  $\blacksquare$

**Remark 5:** Once the attacker can compromise one link  $(i, j) \in \varepsilon_c$ , any NTU attack with nonzero  $\bar{\mathbf{d}}_j^a$  can destabilize the DCmG. Moreover, if the attacker can compromise multi-links  $(i, j) \in \bar{\varepsilon}_a$  cooperatively, then she/he can cause precise impacts (e.g., economic losses) by manipulating the average PCC voltage/output currents.

## 6 Corresponding Countermeasure

In this section, we provide the countermeasure against NTU and ZTU attacks based on encrypted communication network  $\mathcal{G}_{ec}$ , through which the confidentiality and integrity of transmission data can be assured [20]. The countermeasure is composed of attack detection and impact counteraction two phases.

### 6.1 Attack Detection Phase

Since most ZTU and NTU attacks cause steady state average PCC voltage deviation, we aim to detect the attacks by observing the average PCC voltage deviation through the proportional integral average dynamics consensus (PIADC) based estimators deployed in DGUs. Then, the detection indicator  $d_i(t)$  is derived from the estimated average PCC voltage deviation, and certain detection threshold is chosen to tolerate the fluctuations caused by daily operations, e.g., load switches and plugging-in/out of DGUs.

#### 6.1.1 PIADC-based Estimator

According to [21], PIADC-based estimator in DGU  $i$  is

$$\bar{v}_i(s) = h(s)u_1(s), \zeta_i(s) = g(s)u_2(s), \quad (26)$$

where  $h(s) = \frac{\gamma}{s+\gamma}$ ,  $g(s) = \frac{\gamma}{s}$ ,  $u_1(t) = \tilde{V}_i(t) - K_P \sum_{j \in \mathcal{N}_i^{ec}} a_{ij}^{ec}(\bar{v}_i(t) - \bar{v}_j(t)) - K_I \sum_{j \in \mathcal{N}_i^{ec}} a_{ij}^{ec}(\zeta_i(t) - \zeta_j(t))$ ,  $u_2(t) = K_I \sum_{j \in \mathcal{N}_i^{ec}} a_{ij}^{ec}(\bar{v}_i(t) - \bar{v}_j(t))$ . Note that  $\bar{v}_i(t), \zeta_i(t) \in \mathbb{R}$  are transmitted over  $\mathcal{G}_{ec}$ ,  $\bar{v}_i(t)$  is the estimated average PCC voltage, and  $\gamma, K_P, K_I$  are positive gains invariant in all DGUs. Given Theorems 1-2 in [21] and Assumption 2,  $\bar{v}_i(t)$  can track constant and ramp average PCC voltage  $\langle \bar{v}(t) \rangle$  regardless of the initial states  $\bar{v}_i(0), \zeta_i(0)$  with certain  $\gamma, K_P, K_I, a_{ij}^{ec}$ . Therefore, under single and cooperative NTU attacks (20), we always have

$$\bar{\mathbf{v}}(\infty) = \langle \bar{\mathbf{v}}(\infty) \rangle \mathbf{1}^N, \quad (27)$$

where  $\bar{\mathbf{v}}(\infty) = [\bar{v}_1(\infty), \dots, \bar{v}_N(\infty)]^T$ . Moreover, since the encryption and decryption processes are time-consuming due to limited computation capability of each DGU, we aim to encrypt/decrypt only the PIADC-related data to balance the trade off between security and performance of the DCmG.

#### 6.1.2 Sliding Time Window (STW) based Detector

The estimated average PCC voltage deviation is

$$v_i^{err}(t) = V_{ref} - \bar{v}_i(t). \quad (28)$$

Although daily operations in the DCmG never cause nonzero  $v_i^{err}(\infty)$ , non-trivial instantaneous value of

$v_i^{err}(t)$  will emerge as it takes some time for  $\bar{v}_i(t)$  to converge as Fig.3 shows. And it is difficult to distinguish attacks from daily operations based only on  $v_i^{err}(t)$ , which means daily operations may cause non-neglectable false alarms. Therefore, we aim to flatten the fluctuations caused by daily operations based on sliding time window technology and yield the detection indicator  $d_i(t)$ :

$$d_i(t) = \int_{t-T}^t |v_i^{err}(\tau)| d\tau, t \geq t_s + T, \quad (29)$$

where  $T$  is the fixed length of sliding time window,  $t = t_s$  is the activation time, and  $d_i(t)$  calculates the integral of the sliding time window over  $|v_i^{err}(t)|$ . And the generation algorithm of  $d_i(t)$  is shown in Appendix F of [x]. Then, a detection threshold is chosen to tolerate certain daily operations, and the trigger condition of attack alarm is

$$d_i(t) \geq T\Delta_v, \quad (30)$$

where  $\Delta_v > 0$  denotes the least steady state average PCC voltage deviation that can be detected after tolerating daily operations. Obviously,  $\Delta_v$  need cover the maximal average of the integral of the sliding time window over  $|v_i^{err}(t)|$  caused by daily operations, which can be far smaller than the maximum of  $|v_i^{err}(t)|$  if  $T$  is big enough, and thus  $d_i(t)$  can decrease the number of missed alarms caused by tolerating daily operations.

### 6.2 Impact Counteraction Phase

Once (30) is triggered at  $t = T_i^{alm}$ , the estimated average PCC voltage deviation is fed into a PI-based compensator:

$$C_i(t) = k_{cp}v_i^{err}(t) + k_{ci} \int_{T_i^{alm}}^t v_i^{err}(\tau) d\tau, \forall i \in \nu, \quad (31)$$

where  $k_{cp}, k_{ci}$  are positive gains, and  $C_i(t)$  is added to the secondary control input  $\tilde{\psi}_i(t)$ . Therefore, (21) is rewritten as  $\langle \bar{\mathbf{v}}(t) \rangle = V_{ref} + \langle \boldsymbol{\psi}_a(t) \rangle + \langle \mathbf{C}(t) \rangle$ , where  $\mathbf{C}(t) = [C_1(t), \dots, C_N(t)]^T$ . Given (27) and (28), we get  $v_i^{err}(\infty) = -\langle \boldsymbol{\psi}_a(\infty) \rangle - \langle \mathbf{C}(\infty) \rangle$ . If  $\langle \boldsymbol{\psi}_a(\infty) \rangle$  is a constant, then the equilibrium of (31) is achieved with  $|v_i^{err}(\infty)| = 0$ , i.e., voltage balancing is reestablished; If  $\langle \boldsymbol{\psi}_a(\infty) \rangle$  is a ramp signal, then the equilibrium of (31) is achieved with nonzero constant  $|v_i^{err}(\infty)|$ , indicating that voltage balancing cannot be reestablished. Therefore, we aim to identify and cut off threatening communication links  $(i, j) \in \varepsilon_c$  with nonzero  $\bar{\mathbf{d}}_j^a$ . Under Assumption 2, all output currents  $I_{ij}(t), \forall j \in \mathcal{N}_i^c$  are retransmitted from DGU  $j$  to  $i$  through  $\mathcal{G}_{ec}$  to verify the integrity of  $\mathbf{ky}_{i,j}^c(t)$  after (31) has been activated for  $T_c$  long, i.e.,

$$|I_{ij}(t) - \mathbf{ky}_{i,j}^c(t - \tau_{ec})| > \Delta_I, t \geq T_i^{alm} + T_c, \quad (32)$$

where  $\tau_{ec}$  approximates the time delay caused by encryption/decryption processes and  $\Delta_I > 0$  is a predefined threshold to tolerate the exponentially decaying attack vectors<sup>3</sup>. Once (32) is triggered, threatening communication links and corresponding power lines are both cut

<sup>3</sup> According to (20),  $\phi_{i,j}(t)$  decays exponentially to zero if  $\bar{\mathbf{d}}_j^a = \mathbf{0}^2$ .

off to guarantee the establishment of Assumption 1. If  $\mathcal{G}_c$  and  $\mathcal{G}_{el}$  are still connected after cutting off all threatening communication links, then current sharing and voltage balancing can be both reestablished. Furthermore, the counteraction actions (31),(32) are terminated once  $d_i(t) \leq T\delta, t \geq T_i^{comp}$  is achieved, where  $\delta$  is a pre-defined threshold to tolerate the oscillating input  $\tilde{V}_i(t)$ , and  $C_i(T_i^{comp})$  is added to the secondary control input as a constant.

**Remark 6:** Although the countermeasure is designed given the constant  $\bar{d}_j^a(t)$ , we believe that it still works when  $\bar{d}_j^a(t)$  is not constant. We discuss two cases as follows: **1.** if  $\bar{d}_j^a(t)$  decays exponentially to zero, then  $\phi_{i,j}(t)$  will also decay exponentially to zero according to (17), under which current sharing can be achieved while voltage balancing is not achieved with constant average PCC voltage deviation. And the attack impacts can be totally counteracted by (31) without triggering (32). **2.** if  $\bar{d}_j^a(t)$  is a sine/cosine signal, then  $\phi_{i,j}(t)$  will also vary as the sine/cosine signal, under which neither current sharing nor voltage balancing can be achieved. Moreover,  $\langle \bar{v}(t) \rangle$  can only track  $\langle \tilde{v}(t) \rangle \mathbb{1}^N$  with certain tracking error as  $\langle \tilde{v}(t) \rangle$  varies quickly, and the attack impacts can be counteracted only after all threatening communication links with nonzero  $\bar{d}_j^a(t)$  are cut off through (32).

## 7 Simulations

In simulations, we establish a DCmG composed of 8 DGUs in Matlab Simulink/PLECS, and the parameters are given in Appendix C. The nominal reference voltage is  $V_{ref} = 48V$ , and the bounds of noise are  $\bar{\rho}_i = \bar{\omega}_i = [0.001, 0.003, 0]^T, \forall i \in \nu = \{1, 2, \dots, 7, 8\}$ . The simulations are composed of 3 stages:

**Stage 1 (Initialization of DCmG):** At  $t = 0s$ , all primary controllers are activated; At  $t = 2s$ , all DGUs except DGU 7 are connected through power lines; At  $t = 4s$ ,  $\mathcal{G}_c$  and  $\mathcal{G}_{ec}$  are established, and UIO-based detectors, PIADC-based estimators and SWT-based detectors are all activated. The topology of  $\mathcal{G}_{ec}$  coincides with the topology of  $\mathcal{G}_c$ . The weights of  $\mathcal{G}_c$  are set as Assumption 1 and weights of  $\mathcal{G}_{ec}$  are  $a_{ij}^{ec} = 1, \forall (i, j) \in \varepsilon_{ec}$ , and  $k_I = 5$ . The UIO parameters are given in appendix E. Furthermore, constant time delays  $\tau_c = 5ms, \tau_c + \tau_{ec} = 15ms$  are added into  $\mathcal{G}_c$  and  $\mathcal{G}_{ec}$  to simulate transmission and encryption/decryption processes, respectively. Parameters of PIADC-based estimators are  $\gamma = 90, K_P = 3.34$  and  $K_I = 8$ , parameters of STW-based detector are  $T = 1.3s, \Delta_v = 0.4V, \delta = 0.005V$ , and parameters of impact counteraction actions (31),(32) are  $k_{cp} = 1, k_{ci} = 20, T_c = 1s, \Delta_I = 0.1A$ .

**Stage 2 (Daily operations):** At  $t = 8s$ , DGU 8 is disconnected from the DCmG. At  $t = 12s$ , all load currents are decreased by 10% of their rated values. At  $t = 16s$ , DGUs 7 and 8 are plugged into the DCmG simultaneously. According to Fig. 3, the three daily operations will not destroy voltage balancing or current sharing in the DCmG, but they indeed cause some fluctuations on

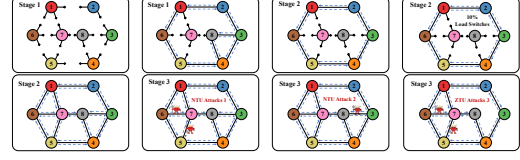


Fig. 2. This figure shows Evolutions of the DCmG, where solid black lines are power lines between DGUs and dotted blue lines denote communication links  $\varepsilon_c$ .

$v_i^{err}(t)$ , and  $\max_{4 \leq t \leq 20, i \in \nu} |v_i^{err}(t)| = 4.7V$ . While the fluctuations on  $d_i(t)$  can be tolerated by  $T\Delta_v$  with the cost of missed alarms for steady state average PCC voltage deviation less than  $\Delta_v = 0.4V < 4.7V$ , indicating that  $d_i(t)$  can effectively decrease the number of false alarms caused by tolerating the daily operations.

**Stage 3 (ZTU/NTU attacks):** At  $t = T_{a1} = 20s$ , NTU attacks 1 targeting at communication links (7,6) and (5,7) are launched, and attack vectors related parameters are  $\bar{d}_6^{a1} = \bar{d}_7^{a1} = \mathbb{0}^2, \phi_{7,6}(T_{a1}) = -0.172 * [1, 0, 1]^T, \phi_{5,7}(T_{a1}) = -0.0337 * [1, 0, 1]^T$ . At  $t = T_{a2} = 25s$ , NTU attack 2 targeting at communication link (8,3) is launched, and the attack vector related parameters are  $\bar{d}_3^{a2} = [-5, 0]^T, \phi_{8,3}(T_{a2}) = -0.0295 * [1, 0, 1]^T$ . At  $t = T_{a3} = 38s$ , ZTU attacks 3 targeting at communication links (7,6) and (5,7) are launched, and attack vectors related parameters are  $\bar{d}_6^{a3} = [0, -0.8333]^T, \bar{d}_7^{a3} = [-10, 0]^T, \phi_{7,6}(T_{a3}) = -0.175 * [1, 0, 1]^T, \phi_{5,7}(T_{a3}) = -0.0343 * [1, 0, 1]^T$ . Note that all initial states of the NTU attacks satisfy (18), and ZTU attacks 3 satisfy  $\sum_{(i,j) \in \varepsilon_a} C_{ij}^a k \phi_{i,j}(\infty) = 0$ . As shown in Fig.4, no attack alarm is triggered by the UIO-based detectors. And according to Fig.3, the impacts of NTU attacks 1 are totally counteracted by the PI-based compensator (31), and voltage balancing is reestablished after  $t = 22.47s$ . NTU attack 2 is detected by DGU 8 at  $T_8^{alm2} = 26.42s$ , and voltage balancing and current sharing are reestablished after  $t = 36.69s$ . ZTU attacks 3 are detected by DGUs 7 and 5 at  $T_7^{alm3} = 38.7s, T_5^{alm3} = 38.76s$ , respectively, and voltage balancing and current sharing are reestablished after  $t = 45.5s$ . Moreover, (32) is not activated by NTU attack 1 as the attack vectors decay exponentially to zero, and is activated by NTU attack 2 and ZTU attacks 3 because of their nonzero  $\bar{d}_j^a$ .

## 8 Conclusion

In this paper, we revealed that the fundamental limitation of UIO-based detector lies in the unknown inputs, which can expose DCmG to the threats of ZTU and NTU attacks. And it is proved that single NTU attack and cooperative NTU attacks can easily destroy current sharing and voltage balancing in the DCmG. Moreover, the proposed countermeasure can detect ZTU and NTU attacks and counteract the attack impacts effectively.

However, there exists several limitations for the proposed countermeasure. First, according to Theorem 4, cooperative NTU attacks satisfying (25) can destroy cur-

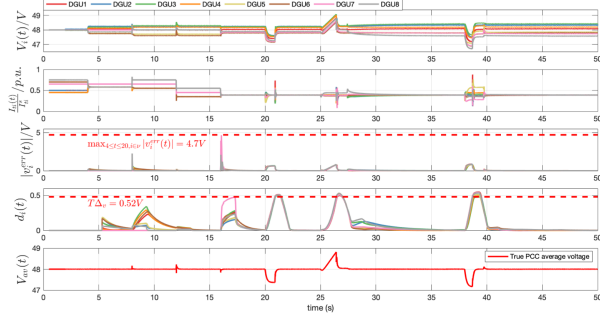


Fig. 3. This figure shows the evolution of PCC voltages  $V_i(t)/V$ , output currents in per-unit  $I_{i_s}^d(t)/p.u.$ , estimated average PCC voltage  $\bar{v}_i(t)$ , detection indicators  $d_i(t)$  and the true average PCC voltage  $V_{av}(t)$  under daily operations and attacks. The red dotted lines in  $|v_i^{err}(t)|$  and  $d_i(t)$  denote  $\max_{4 \leq t \leq 20, i \in \nu} |v_i^{err}(t)|$  and  $T\Delta_v$ , respectively.

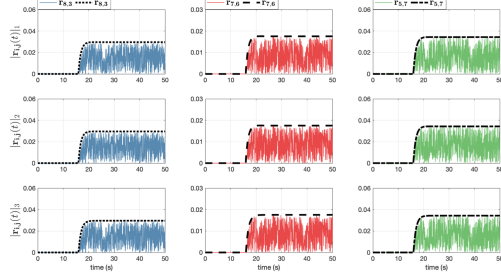


Fig. 4. This figure shows the evolution of residuals  $|r_{8,3}(t)|$ ,  $|r_{7,6}(t)|$  and  $|r_{5,7}(t)|$ ,  $t \geq 16$ , where solid lines represent the real residuals, dotted lines represent the bounds of residuals, and  $|r_{i,j}(t)|_a$  represents the  $a_{th}$  entry.

rent sharing with small average PCC voltage deviation, which means the proposed countermeasure may not detect and counteract these attacks. Second, the impact counteraction phase requires to cut off all threatening communication links with nonzero  $\bar{d}_j^a$ , which not only can eliminate attack vectors but also will degrade control performances a lot and even disconnect  $\mathcal{G}_c$ . Therefore, it is necessary to detect the undetectable attacks under the UIO-based detector based on the average PCC voltage deviation and output currents, simultaneously, and the attack impacts may be counteracted by estimating the attack vectors through the encrypted network, which are left for our future works.

## References

- [1] M. Liu, C. Zhao, R. Deng, P. Cheng, W. Wang, and J. Chen, "Nonzero-dynamics stealthy attack and its impacts analysis in dc microgrids," in *2019 American Control Conference (ACC)*. IEEE, 2019, pp. 3922–3927.
- [2] N. Hatziargyriou, *Microgrids: architectures and control*. John Wiley & Sons, 2014.
- [3] M. Tucci, S. Rivero, J. C. Vasquez, J. M. Guerrero, and G. Ferrari-Trecate, "A decentralized scalable approach to voltage control of dc islanded microgrids," *IEEE Transactions on Control Systems Technology*, vol. 24, no. 6, pp. 1965–1979, 2016.
- [4] M. Tucci, L. Meng, J. M. Guerrero, and G. Ferrari-Trecate, "Stable current sharing and voltage balancing in

dc microgrids: A consensus-based secondary control layer," *Automatica*, vol. 95, pp. 1–13, 2018.

- [5] V. Nasirian, S. Moayedi, A. Davoudi, and F. L. Lewis, "Distributed cooperative control of dc microgrids," *IEEE Transactions on Power Electronics*, vol. 30, no. 4, pp. 2288–2303, 2015.
- [6] M. Hossain, H. R. Pota, M. A. Mahmud, and M. Aldeen, "Robust control for power sharing in microgrids with low-inertia wind and pv generators," *IEEE Transactions on Sustainable Energy*, vol. 6, no. 3, pp. 1067–1077, 2015.
- [7] T. Ding, Y. Lin, Z. Bie, and C. Chen, "A resilient microgrid formation strategy for load restoration considering master-slave formation distributed generators and topology reconfiguration," *Applied energy*, vol. 199, pp. 205–216, 2017.
- [8] L.-Y. Lu, H. J. Liu, and H. Zhu, "Distributed secondary control for isolated microgrids under malicious attacks," in *North American Power Symposium (NAPS)*. IEEE, 2016, pp. 1–6.
- [9] H. J. Liu, M. Backes, R. Macwan, and A. Valdes, "Coordination of ders in microgrids with cybersecure resilient decentralized secondary frequency control," in *Proceedings of the 51st Hawaii International Conference on System Sciences (HICSS)*, 2018, pp. 2670–2679.
- [10] O. A. Beg, T. T. Johnson, and A. Davoudi, "Detection of false-data injection attacks in cyber-physical dc microgrids," *IEEE Transactions on Industrial Informatics*, vol. 13, no. 5, pp. 2693–2703, 2017.
- [11] A. Teixeira, H. Sandberg, and K. H. Johansson, "Networked control systems under cyber attacks with applications to power networks," in *Proceedings of the 2010 American Control Conference*. IEEE, 2010, pp. 3690–3696.
- [12] A. J. Gallo, M. S. Turan, P. Nahata, F. Boem, T. Parisini, and G. Ferrari-Trecate, "Distributed cyber-attack detection in the secondary control of dc microgrids," in *2018 European Control Conference (ECC)*. IEEE, 2018, pp. 344–349.
- [13] T. M. Chen, "Stuxnet, the real start of cyber warfare?[editor's note]," *IEEE Network*, vol. 24, no. 6, pp. 2–3, 2010.
- [14] X. Ge, Q.-L. Han, and F. Yang, "Event-based set-membership leader-following consensus of networked multi-agent systems subject to limited communication resources and unknown-but-bounded noise," *IEEE Transactions on Industrial Electronics*, vol. 64, no. 6, pp. 5045–5054, 2016.
- [15] J. M. Bravo, A. Suarez, M. Vasallo, and T. Alamo, "Slide window bounded-error time-varying systems identification," *IEEE Transactions on Automatic control*, vol. 61, no. 8, pp. 2282–2287, 2015.
- [16] M. Crosbie and E. H. Spafford, "Defending a computer system using autonomous agents," *Technical Reporter 95-022, COAST Laboratory-Purdue University*, 1994.
- [17] J. Chen, R. J. Patton, and H.-Y. Zhang, "Design of unknown input observers and robust fault detection filters," *International Journal of Control*, vol. 63, no. 1, pp. 85–105, 1996.
- [18] G. Basile and G. Marro, *Controlled and conditioned invariants in linear system theory*. Prentice Hall Englewood Cliffs, NJ, 1992.
- [19] F. Pasqualetti, F. Dörfler, and F. Bullo, "Attack detection and identification in cyber-physical systems," *IEEE transactions on automatic control*, vol. 58, no. 11, pp. 2715–2729, 2013.
- [20] E. Chikuni and M. Dondo, "Investigating the security of electrical power systems scada," in *AFRICON 2007*. IEEE, 2007, pp. 1–7.

- [21] H. Bai, R. A. Freeman, and K. M. Lynch, "Robust dynamic average consensus of time-varying inputs," in *49th IEEE Conference on Decision and Control (CDC)*. IEEE, 2010, pp. 3104–3109.
- [22] R. Olfati-Saber and R. M. Murray, "Consensus problems in networks of agents with switching topology and time-delays," *IEEE Transactions on automatic control*, vol. 49, no. 9, pp. 1520–1533, 2004.
- [23] X.-D. Zhang, "The laplacian eigenvalues of graphs: a survey," *arXiv preprint arXiv:1111.2897*, 2011.

## A Proof of Theorem 3

**Proof:** According to Proposition 3 in [4], we have a)  $\ker(\mathbf{Q}) = \mathbb{H}_\perp^1$ ,  $\text{range}(\mathbf{Q}) = \mathbb{H}^1$ ; b)  $\mathbf{Q}$  is diagonalizable and has non-negative eigenvalues, and its algebraic multiplicity of zero eigenvalue is one. Therefore, the eigenvalue eigenvector pairs of  $\mathbf{Q}$  can be denoted by  $\mathbf{p}_i = (\lambda_i, \mathbf{q}_i)$ ,  $i \in \mathcal{V}$ , where  $\lambda_1 = 0$ ,  $0 < \lambda_2 \leq \dots \leq \lambda_N$ ,  $\mathbf{q}_i \in \mathbb{R}^N$ ,  $\mathbf{q}_1 \in \mathbb{H}_\perp^1$ , and  $\{\mathbf{q}_2, \dots, \mathbf{q}_N\}$  constitutes a basis of  $\mathbb{H}^1$ . Thus, in the absence of (20), we have

$$\psi(t) = e^{-\mathbf{Q}t} \psi(0) + \sum_{i=2}^N \frac{\alpha_i}{\lambda_i} (1 - e^{-\lambda_i t}) \mathbf{q}_i, \quad (\text{A.1})$$

where  $\alpha_i \in \mathbb{R}$  and  $\sum_{i=2}^N \alpha_i \mathbf{q}_i = -\tilde{\mathbf{L}} \mathbf{D} \mathbf{i}_l - \mathbf{Q} \mathbf{v}_{ref} \in \mathbb{H}^1$ . If  $\psi(0) \in \mathbb{H}^1$ , then  $\langle \psi(\infty) \rangle = 0$  and voltage balancing and current sharing can be achieved at exponential convergence rate  $\lambda_2$ . And we let  $\psi_a(t) = \psi_{a1}(t) + \psi_{a2}(t)$ , where  $\psi_{a1}(t)$ ,  $\psi_{a2}(t)$  represent the attack impacts caused by  $e^{\mathbf{A}_{kj}(t-T_a)} \tilde{\phi}_{i,j}(T_a)$  and  $-\mathbf{A}_{kj}^{-1} \bar{\mathbf{E}}_j \bar{\mathbf{d}}_j^a$ , respectively. As  $\mathbf{A}_{kj}^{-1} \bar{\mathbf{E}}_j \bar{\mathbf{d}}_j^a$  is a constant,  $\psi_{a2}(t)$  can be directly obtained as

$$\psi_{a2}(t) = \alpha_{1l}(t - T_a) \mathbf{q}_1 + \sum_{i=2}^N \frac{\alpha_{il}}{\lambda_i} (1 - e^{-\lambda_i(t-T_a)}) \mathbf{q}_i, \quad (\text{A.2})$$

where  $\alpha_{il} \in \mathbb{R}$  and  $\sum_{i=1}^N \alpha_{il} \mathbf{q}_i = -C_{ij}^a \mathbf{k} \mathbf{A}_{kj}^{-1} \bar{\mathbf{E}}_j \bar{\mathbf{d}}_j^a \mathbf{l}_i$ . If  $\mathbf{A}_{kj}$  is diagonalizable<sup>4</sup>, then we have  $e^{\mathbf{A}_{kj}(t-T_a)} \tilde{\phi}_{i,j}(T_a) = \sum_{m=1}^3 \eta_m e^{\beta_m(t-T_a)} \mathbf{a}_m$ , where  $(\beta_m, \mathbf{a}_m)$ ,  $\forall m \in \mathcal{V} = \{1, 2, 3\}$  are the eigenvalue eigenvector pairs of  $\mathbf{A}_{kj}$ ,  $\eta_m \in \mathbb{R}$ ,  $\mathbf{a}_m \in \mathbb{R}^3$  and  $\sum_{m=1}^3 \eta_m \mathbf{a}_m = \tilde{\phi}_{i,j}(T_a)$ . Thus,

$$\psi_{a1}(t) = \sum_{m=1}^3 \tilde{C}_{ij}^a e^{-\beta_m T_a} e^{-\mathbf{Q}t} \int_{T_a}^t e^{\beta_m \tau} e^{\mathbf{Q}\tau} \mathbf{l}_i d\tau, \quad (\text{A.3})$$

where  $\tilde{C}_{ij}^a = C_{ij}^a \eta_m a_{m2} \in \mathbb{R}$  and  $a_{m2} = \mathbf{k} \mathbf{a}_m \in \mathbb{R}$ . As  $\{\mathbf{q}_1, \mathbf{q}_2, \dots, \mathbf{q}_N\}$  constitutes a basis of  $\mathbb{R}^N$ ,  $\mathbf{l}_i$  can be decomposed as  $\mathbf{l}_i = \sum_{r=1}^N \delta_r \mathbf{q}_r$ , where  $\delta_1 \mathbf{q}_1 = \langle \mathbf{l}_i \rangle \mathbb{1}^N = \frac{1}{N} \mathbb{1}^N$ , and thus  $e^{\mathbf{Q}t} \mathbf{l}_i = \sum_{r=1}^N \delta_r e^{\lambda_r t} \mathbf{q}_r$ . If  $\beta_m + \lambda_r \neq$

$0, \forall m \in \mathcal{V}, r \in \mathcal{V}$ ,<sup>5</sup> then the integral part in (A.3) can be computed as

$$\int_{T_a}^t e^{\beta_m \tau} e^{\mathbf{Q}\tau} \mathbf{l}_i d\tau = \sum_{r=1}^N \frac{\delta_r}{\beta_m + \lambda_r} (e^{(\beta_m + \lambda_r)t} - e^{(\beta_m + \lambda_r)T_a}) \mathbf{q}_r. \quad (\text{A.4})$$

Substituting (A.4) into (A.3), we get

$$\psi_{a1}(t) = \sum_{m=1}^3 \sum_{r=1}^N \frac{C_a \eta_m a_{m2} \delta_r}{\beta_m + \lambda_r} (e^{\beta_m(t-T_a)} - e^{-\lambda_r(t-T_a)}) \mathbf{q}_r.$$

Given (A.2) and  $\alpha_{1l} \mathbf{q}_1 = \frac{k_I a_{ij}}{N I_{tj}^s} \mathbf{k} \mathbf{A}_{kj}^{-1} \bar{\mathbf{E}}_j \bar{\mathbf{d}}_j^a \mathbb{1}^N$ , we have

$$\langle \psi_{a2}(\infty) \rangle = \frac{k_I a_{ij}}{N I_{tj}^s} \mathbf{k} \mathbf{A}_{kj}^{-1} \bar{\mathbf{E}}_j \bar{\mathbf{d}}_j^a (t - T_a). \quad (\text{A.5})$$

Since  $\mathbf{A}_{kj}$  is stable,  $Re(\beta_m) < 0, \forall m \in \mathcal{V}$ . And given the expression of  $\psi_{a1}(t)$  and  $\delta_1 \mathbf{q}_1 = \frac{1}{N} \mathbb{1}^N$ , we get

$$\langle \psi_{a1}(\infty) \rangle = - \sum_{m=1}^3 \frac{C_a \eta_m a_{m2}}{N \beta_m}. \quad (\text{A.6})$$

Moreover, as  $(\frac{1}{\beta_m}, \mathbf{a}_m)$ ,  $\forall m \in \mathcal{V}$  are the eigenvalue eigenvector pairs of  $\mathbf{A}_{kj}^{-1}$ , we have

$$e^{\mathbf{A}_{kj}^{-1}(t-T_a)} \tilde{\phi}_{i,j}(T_a) = \sum_{m=1}^3 \eta_m e^{\frac{1}{\beta_m}(t-T_a)} \mathbf{a}_m. \quad (\text{A.7})$$

After differentiating (A.7) and letting  $t = T_a$ , we obtain

$$\mathbf{A}_{kj}^{-1} \tilde{\phi}_{i,j}(T_a) = \sum_{m=1}^3 \frac{\eta_m}{\beta_m} \mathbf{a}_m. \quad (\text{A.8})$$

Substituting (A.8) into (A.6), we get

$$\langle \psi_{a1}(\infty) \rangle = - \frac{k_I a_{ij}}{N I_{tj}^s} \mathbf{k} \mathbf{A}_{kj}^{-1} \tilde{\phi}_{i,j}(T_a). \quad (\text{A.9})$$

Adding (A.5) and (A.9), we can get the total attack impacts

$$\langle \psi_a(\infty) \rangle = \frac{k_I a_{ij}}{N I_{tj}^s} \mathbf{k} \mathbf{A}_{kj}^{-1} ((t - T_a) \bar{\mathbf{E}}_j \bar{\mathbf{d}}_j^a - \tilde{\phi}_{i,j}(T_a)).$$

Since  $\langle \psi(t) \rangle$  decays exponentially to zero and  $\langle \psi_a(t) \rangle$  diverges with  $t$ ,  $\langle \tilde{\psi}(t) \rangle$  also diverges with  $t$  given  $\langle \tilde{\psi}(t) \rangle = \langle \psi(t) \rangle + \langle \psi_a(t) \rangle$ . Moreover, according to (21),  $\langle \tilde{\mathbf{v}}(t) \rangle$  also diverges with  $t$ , i.e., voltage balancing is not achieved. Meanwhile, given (A.2), each entry in  $\psi_{a2}(t)$  diverges with  $t$ , indicating that all PCC voltages, including the DGUs whose communication links are not attacked, cannot converge. Therefore, we can infer that current sharing is not achieved either, which completes the proof. ■

<sup>5</sup> When  $\beta_m = -\lambda_r$ , the integral part in (A.4) will be differentiated, and the system can still achieve convergence but not at an exponential speed.

<sup>4</sup> When  $\mathbf{A}_{kj}$  is not diagonalizable, the stability and convergence properties can be analyzed in a similar way, under which system states can still converge to a stable value but not at an exponential speed.

## B Proof of Theorem 4

**Proof:** According to (20),  $\phi_{i,j}(\infty) = -\mathbf{A}_{kj}^{-1} \bar{\mathbf{E}}_j \bar{\mathbf{d}}_j^a$ , indicating that

$$\sum_{(i,j) \in \bar{\mathcal{E}}_a} C_{ij}^a \mathbf{k} \mathbf{A}_{kj}^{-1} \bar{\mathbf{E}}_j \bar{\mathbf{d}}_j^a = 0. \quad (\text{B.1})$$

Substituting (B.1) into (24), we get

$$\langle \psi_a(\infty) \rangle = - \sum_{(i,j) \in \bar{\mathcal{E}}_a} \frac{C_{ij}^a}{N} \mathbf{k} \mathbf{A}_{kj}^{-1} \tilde{\phi}_{i,j}(T_a), \quad (\text{B.2})$$

which means that the average PCC voltage finally converges.

*Voltage Balancing:* The steady state average PCC voltage under attack is

$$\langle \tilde{\mathbf{v}}(\infty) \rangle = V_{ref} + \langle \psi_a(\infty) \rangle. \quad (\text{B.3})$$

According to Definition 1, voltage balancing is achieved if  $\sum_{(i,j) \in \bar{\mathcal{E}}_a} \frac{C_{ij}^a}{N} \mathbf{k} \mathbf{A}_{kj}^{-1} \tilde{\phi}_{i,j}(T_a) = 0$ .

*Current Sharing:* Given (22), when  $\tilde{\psi}(t)$  achieves the equilibrium, we have

$$\tilde{\mathbf{L}} \mathbf{D} \tilde{\mathbf{i}}_t(\infty) = \sum_{(i,j) \in \bar{\mathcal{E}}_a} C_{ij}^a \mathbf{k} \phi_{i,j}(\infty) \mathbf{l}_i. \quad (\text{B.4})$$

Given (B.1), we obtain  $\langle \sum_{(i,j) \in \bar{\mathcal{E}}_a} C_{ij}^a \mathbf{k} \phi_{i,j}(\infty) \mathbf{l}_i \rangle = \mathbf{0}^N$ , indicating that (B.4) is solvable. And the solution  $\tilde{\mathbf{i}}_t(\infty) \in \mathbb{H}_\perp^1$ , which is equivalent to current sharing in the DCmG, if  $\sum_{(i,j) \in \bar{\mathcal{E}}_a} C_{ij}^a \mathbf{k} \phi_{i,j}(\infty) \mathbf{l}_i = \mathbf{0}^N$ . Therefore, the proof is completed. ■

## C Parameters of DGUs

## D Time Delay Margin

**Remark 7:** Furthermore, we have further investigated the relationship between the time delay margin of the PIADC-based estimator and the PIADC parameters and  $\lambda_N^e$ , i.e., the maximal eigenvalue of  $\mathbf{L}_e$ . As shown in Tables D.1-D.2, smaller PIADC parameters have larger time delay margin and larger  $\lambda_N^e$  causes smaller time delay margin, which matches the result of Theorem 10 in [22]. According to Theorem 3.20 in [23], the lower bound of  $\lambda_N^e$  is positively related to the number of edges if  $|\varepsilon_{ec}| < \frac{N(N-1)}{4}$ . Therefore, higher edge-connectivity of  $\mathcal{G}_{ec}$ <sup>6</sup> causes smaller time delay margin

<sup>6</sup> The minimum number of edges whose removal renders  $\mathcal{G}_{ec}$  disconnected.

Table C.1  
Electrical Parameters of DGUs

Converter parameters							
DGU	$R_t(\Omega)$	$L_t(mH)$	$C_t(mF)$	DGU	$R_t(\Omega)$	$L_t(mH)$	$C_t(mF)$
DGU1	0.2	1.8	2.2	DGU2	0.4	2.0	1.7
DGU3	0.3	2.2	1.9	DGU4	0.6	2.5	2.4
DGU5	0.5	3.0	2.7	DGU6	0.4	1.6	3.0
DGU7	0.2	1.4	2.1	DGU8	0.4	1.2	1.6

Power line parameters							
$(i,j)$	$R_{ij}(\Omega)$	$(i,j)$	$R_{ij}(\Omega)$	$(i,j)$	$R_{ij}(\Omega)$	$(i,j)$	$R_{ij}(\Omega)$
(1,2)	0.05	(1,6)	0.10	(2,3)	0.07	(3,4)	0.09
(3,8)	0.12	(4,5)	0.14	(4,8)	0.20	(5,6)	0.25
(5,7)	0.06	(6,7)	0.10	(1,7)	0.15	(8,7)	0.17

Table C.2  
Load Currents of DGUs

Converter parameters					
DGU	$I_{Li}(A)$	$L_{ti}^s(A)$	DGU	$I_{Li}(A)$	$L_{ti}^s(A)$
DGU1	10	20	DGU2	10	20
DGU3	15.75	30	DGU4	9	20
DGU5	14	20	DGU6	21	30
DGU7	16.25	25	DGU8	18.75	25

if  $|\varepsilon_{ec}| < \frac{N(N-1)}{4}$ . Moreover,  $\lambda_N^e$  is positively related to the edge weights, and thus larger edge weights lead to smaller time delay margin.

Table D.1  
Time delay margin under different PIADC parameters,  $\lambda_N^e = 5.5616$ .

$\gamma, K_P, K_I$	75, 4, 6.5	85, 6, 8	95, 8, 10	100, 10, 14
Margin(ms)				
Time delay margin	55	35	15	5

Table D.2  
Time delay margin under different  $\lambda_N^e$ ,  $\gamma = 95, K_P = 8, K_I = 10$ .

$\lambda_N^e$	5.4903	.5616	6
Margin(ms)			
Time delay margin	16	15	10.5

## E UIO Parameters

$$\mathbf{F}_3 = \mathbf{F}_6 = \mathbf{F}_7 = \begin{bmatrix} -1 & 0 & 0 \\ 0 & -1 & 0 \\ 0 & 0 & -1 \end{bmatrix}, \mathbf{H}_3 = \begin{bmatrix} 1 & -0.05 & 0 \\ 0 & 0.95 & 0 \\ 0 & -0.05 & 1 \end{bmatrix}.$$

$$\mathbf{H}_6 = \begin{bmatrix} 1 & -0.02 & 0 \\ 0 & 0.98 & 0 \\ 0 & -0.02 & 1 \end{bmatrix}, \mathbf{H}_7 = \begin{bmatrix} 1 & -0.04 & 0 \\ 0 & 0.96 & 0 \\ 0 & -0.04 & 1 \end{bmatrix}.$$

## F Calculation algorithm of $d_i(t)$

Algorithm 1 shows detailed generation process of  $d_i(t)$ , and  $d_i(t)$  is updated every sampling period  $\Delta_t$ . First,  $|v_i^{err}(t)|, t \in \mathbf{S}_T$  are recorded into  $\mathbf{v}_r \in \mathbb{R}^{N_T-1}$  through lines 2-4. The sum of all entries in  $\mathbf{v}_r$  is calculated as  $S_{um}$  at line 5. Then, for each  $v_i^{err}(t), t \geq t_s + T$ , real-time  $d_i(t)$  is calculated as line 8, and  $\mathbf{v}_r, S_{um}$  are updated for next circle through lines 7 and 9-13.

---

### Algorithm 1 Generation of detection indicator $d_i(t)$

---

**Input:** Average PCC voltage deviation,  $v_i^{err}(t), t \geq t_s$ ;  
Sampling period,  $\Delta_t$ ; Length of the sliding window,  
 $T = N_T \Delta_t, N_T \geq 1$ ; Record vector,  $\mathbf{v}_r = \mathbb{0}^{N_T-1}$ .  
**Output:** The detection indicator,  $d_i(t), t \geq t_s, \forall i \in \nu$ ;  
1:  $d_i(t_s) = 0$ ;  
2: **for** each  $t \in \mathbf{S}_T = \{t_s + \Delta_t, \dots, t_s + (N_T - 1)\Delta_t\}$  **do**  
3:      $\mathbf{v}_r((t - t_s)/\Delta_t) = |v_i^{err}(t)|, d_i(t) = 0$ ;  
4: **end for**  
5: Calculate  $S_{um} = \sum_{k=1}^{N_T-1} \mathbf{v}_r(k)$ ;  
6: **for** each  $t \geq t_s + T$  **do**  
7:      $S_{um} = S_{um} + |v_i^{err}(t)|$ ;  
8:      $d_i(t) = \Delta_t S_{um}$ ;  
9:      $S_{um} = S_{um} - \mathbf{v}_r(1)$ ;  
10:    **for**  $k = 1; k < N_T - 1; k = k + 1$ ; **do**  
11:        $\mathbf{v}_r(k) = \mathbf{v}_r(k + 1)$ ;  
12:    **end for**  
13:     $\mathbf{v}_r(N_T - 1) = |v_i^{err}(t)|$ ;  
14: **end for**

---